

Radial Position Sensing in a Coplanar-Grid High-Pressure Xenon Gamma-Ray Spectrometer

Scott D. Kiff, *Student Member, IEEE*, Zhong He, *Senior Member, IEEE*, and Gary C. Tepper

Abstract—This paper describes a technique for determining the interaction radius of a gamma ray within a cylindrical detector. This can be useful information for correcting pulse amplitudes and selecting events of interest. A theoretical expression for the event radius is derived based on anode signals, and simulations are compared with experimental results.

Index Terms—Coplanar anodes, gas detectors, Geant, high-pressure xenon, ionization chambers, position sensing, single polarity charge sensing, .

I. INTRODUCTION

THE interaction position of a gamma ray within a detector is a valuable piece of information to obtain. The interaction location can be used to apply a pulse height correction, to diagnose the detector's operating conditions, and to select interactions of interest within the detector.

In high-pressure xenon (HPXe) ionization chambers, a Frisch grid is typically used to remove the position-dependence of the anode signal amplitude. In these detectors, spectroscopic performance has improved steadily, with energy resolution near 2% full width at half maximum (FWHM) at 662 keV [1]–[3]. Unfortunately, vibration of the Frisch grid in these detectors can severely degrade spectroscopic performance in uncontrolled environments. To combat the potential microphonic problems, there have been efforts to use gridless detectors with a method of correcting the pulse amplitude as a function of interaction radius. Typically this involves measuring the pulse rise time; this rise time can be measured directly from the induced charge on the anode [4], or the scintillation light emitted in the initial ionization cloud can be used as a time stamp [5].

A handful of efforts to determine the interaction position within the detector have been reported in the literature. One method for making such a measurement is to vary the grid-anode spacing in a planar detector geometry, and to use the scintillation light emitted while electrons traverse the grid-anode gap to measure a pulse rise time [6]. The time can then easily be converted into an interaction coordinate. Another reported method is to place several pickup wires outside a

cylindrical HPXe chamber, then use the transient signal on each pickup wire to determine the interaction radius and azimuthal angle [7]. A third approach to measuring interaction position is to actually segment the cathode into strips and then measure the induced signal on each strip, using the signatures left on each cathode strip to determine the interaction radius and azimuthal angle [8].

While determining anode signal rise times, measuring transient signals on the cathode and on pickup wires, and using scintillation light as a time stamp are effective methods of determining the interaction location of a gamma ray within the detector, these methods can be somewhat challenging to employ in practice. The slow drift of electrons through xenon gas makes the beginning and end of the anode signal's rise difficult to determine exactly, and scintillation light collection can be difficult due to problems mating a photomultiplier tube to a high-pressure chamber. Furthermore, the input capacitance for the pickup wire and cathode strip preamplifiers can be large, reducing the signal-to-noise ratio.

This paper explores another alternative to the Frisch grid, the technique of coplanar anode grids first reported by P. N. Luke [9]. In the coplanar anode technique, the detector's anode is segmented in such a way as to form two independent anodes. Usually one of the anodes is biased higher than the other, so that the electrons will always be collected on one anode, labeled the collecting anode; the electrons will induce a transient signal on the second anode, dubbed the noncollecting anode. If the anode is designed and operated optimally, subtracting the noncollecting anode's preamplifier output signal from the collecting anode's will give a final pulse amplitude that is independent of both the interaction location inside the detector and also positive ion motion, although electron-ion recombination must be negligible.

Design and initial operation of a HPXe coplanar anode detector has been reported previously [10]. The two anode signals can be used to give not only the position-independent signal amplitude, but also the approximate radial coordinate of the gamma-ray interaction. This paper will first introduce a theoretical expression for the interaction radius as a function of anode signal amplitudes, then present experimental data, and finally describe detailed simulations that support the experiments.

II. RADIAL SENSING THEORY

To determine the radial position of the interaction within the cylindrical detection volume, let us first explore the weighting potential distribution within the detector, $\varphi(r, \theta, z)$. In this equation, the radial, azimuthal, and axial coordinates are r , θ , and z ,

Manuscript received December 1, 2005; revised April 5, 2006. This work was supported in part by a National Science Foundation Graduate Research Fellowship and in part by the U.S. Department of Energy NEER under Grant DE-FG07-02ID14332.

S. D. Kiff and Z. He are with the University of Michigan, Ann Arbor, MI 48109 USA (e-mail: kiff@umich.edu; hezhong@umich.edu).

G. C. Tepper is with Virginia Commonwealth University, Richmond, VA 23284 USA (e-mail: gtepper@vcu.edu).

Digital Object Identifier 10.1109/TNS.2006.875152

respectively. The weighting potential distribution is governed by Laplace's equation

$$\nabla^2 \varphi(r, \theta, z) = 0. \quad (1)$$

Let us consider a simplified case where axial and azimuthal changes are negligible compared to radial effects. In this case, (1) can be solved to produce (2), which defines the weighting potential for the anodes. In this equation, R_C and R_A denote the radii at which the cathode surface and the anode wires lie, respectively, and $\varphi_S(r)$ is the weighting potential when the two anode responses are summed

$$\varphi_S(r) = \frac{\ln(R_C/r)}{\ln(R_C/R_A)}. \quad (2)$$

Equation (2) describes a function that increases monotonically between the cathode and anodes, which allows for a correlation between the anode signal and the interaction radius. However, the weighting potential is not directly measured—the net induced charge on the anodes is the known quantity. Thus, the Shockley-Ramo theorem [11], which is represented in general form by (3), is used to correlate weighting potential to the induced charge on the anodes, Q . The parameter q is the amount of moving charge created in the interaction, and r_0 denotes the initial position of the charge cloud in the detector

$$Q(r) = -q[\varphi(r) - \varphi(r_0)]. \quad (3)$$

To first approximation, the electron charge created in the detector is given by $-Q_D$, which is the difference of the final collecting and noncollecting anode induced charges, Q_{col} and Q_{non} . This is known from theory supporting the coplanar anode technique

$$-q = Q_{\text{col}} - Q_{\text{non}} = Q_D. \quad (4)$$

It is now a matter of using (2)—(4), along with some algebra, to deduce the radial coordinate of the interaction in terms of the sum of the final anode signals, Q_S , and Q_D

$$\frac{r_0}{R_C} = \left(\frac{R_C}{R_A} \right)^{(Q_S/Q_D)-1}. \quad (5)$$

It is important to quantify the position resolution of the detector. To start, let us assume the anode sum and difference signal noise terms are uncorrelated. We can then employ the error propagation formula

$$\sigma_{r_0}^2 = \left(\frac{\partial r_0}{\partial Q_S} \right)^2 \sigma_S^2 + \left(\frac{\partial r_0}{\partial Q_D} \right)^2 \sigma_D^2. \quad (6)$$

In (6), σ_S , σ_D , and σ_{r_0} are the standard deviations in the distribution of the measured Q_S , Q_D , and r_0 , respectively. Using the

relationship described by (5), it is easy to derive the following relationship for σ_{r_0} :

$$\frac{\sigma_{r_0}}{r_0} = \frac{\ln(R_C/R_A)}{Q_D} \sqrt{\sigma_S^2 + \left(\frac{Q_S}{Q_D} \right)^2 \sigma_D^2}. \quad (7)$$

Let us assume σ_S and σ_D are approximately equal. If the noise on the two anodes is independent, this is a valid assumption: the error propagation formula applied to the sum and difference of the two raw anode signals will then yield the same uncertainty result for σ_S and σ_D . Let us also convert standard deviation to FWHM. We now can determine the position resolution as an approximate function of the energy resolution

$$\frac{\text{FWHM}_{r_0}}{r_0} = \ln \left(\frac{R_C}{R_A} \right) \sqrt{1 + \left(\frac{Q_S}{Q_D} \right)^2} \frac{\text{FWHM}_D}{Q_D}. \quad (8)$$

Examining (8), we expect the position resolution to vary as a function of radius. Events occurring near the anodes will induce a summed signal $Q_S \approx 0$, so the position resolution will simply be the energy resolution multiplied by the geometrical constant. At the other extreme, events near the cathode will be identified by $Q_S \approx Q_D$, so the position resolution will broaden by a factor of $\sqrt{2}$ relative to near-anode events.

III. EXPERIMENTS

The HPXe detector is described in detail in [10], and a schematic appears in Fig. 1; a summary of important parameters can be found in Table I. The detector utilizes a cylindrical geometry, with the cathode forming the outer wall of the sensitive volume and the anode wires lying near the center of the detector. There are a total of 12 anode wires that are stretched axially through the detection volume, and they are arranged symmetrically about the main axis of the detector with uniform radial displacement and interwire spacing. The detector fill gas is purified xenon.

Although there are 12 wires, they are connected into two sets such that neighboring wires belong to opposite groups. Thus, there are 2 independent anode signals, and each anode is connected to an Amptek A250 charge-sensitive preamplifier. The preamplifier output signals have been digitized using an Agilent Infiniium 54825A oscilloscope, and the digitized signals are acquired and recorded to file using LabVIEW [12] on a PC. All post-processing of the data is performed using MATLAB [13].

Data has been collected using ^{137}Cs and ^{57}Co point sources. For all experiments, the cathode bias was held at -4000 V, the noncollecting anode at ground, and the collecting anode at $+1400$ V. Each triggered event was sampled at 400-ns intervals for a total of 500 samples.

With the MATLAB post-processing program, the digitized preamplifier pulses were added and subtracted to get the sum and difference signals; these signals were shaped with a Gaussian filter characterized by a $32\text{-}\mu\text{s}$ shaping time. The normalized radial coordinate of each event was calculated via (5), and events were sorted into several radial bins. The

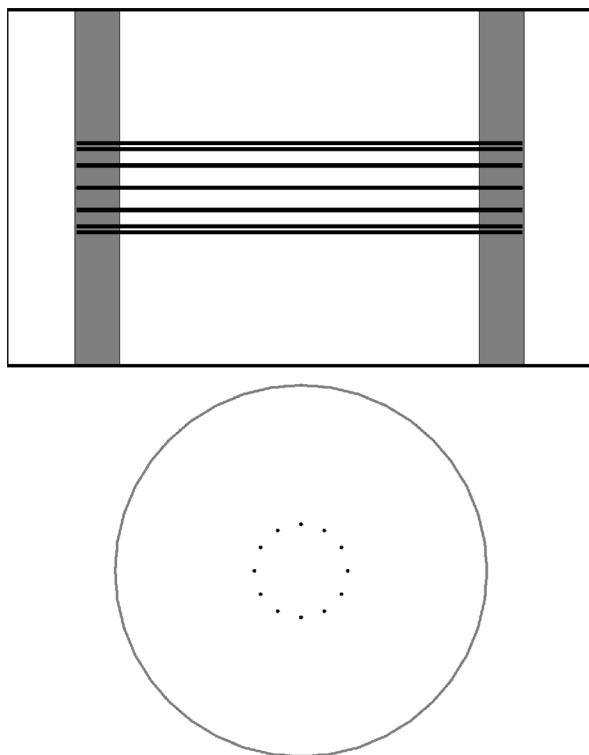


Fig. 1. Simplified cross-sectional schematics of the detector interior; anode wires are black, Macor structural material is dark gray, and white areas are filled with xenon. Top: a side view. Bottom: a cross-sectional view through the active volume.

TABLE I
A SUMMARY OF IMPORTANT DETECTOR PARAMETERS

Parameter	Design Value
Detection volume length	101.6 mm
Cathode diameter	101.6 mm
Anode displacement from central axis	12.7 mm
Anode wire diameter	1.0 mm
Xenon density	0.3 g/cm ³

radially-separated pulse-height spectra for the ¹³⁷Cs source are shown in Fig. 2. In this figure there are several notable features:

1. all counts register outside the anode wires (radius = 0.25);
2. the photopeak becomes better defined as the radius increases;
3. the photopeak seems to disappear at a radius much less than 1.00 (the theoretical cathode radius);
4. there is a significant low-energy continuum for radius ≥ 1.00 ; and
5. electronic noise is significant, measured by the test pulse peak centered near channel 900 in the largest two radial bins.

The significant electronic noise term is explained by the long shaping time used to minimize ballistic deficit problems. The photopeak disappearance is better visualized in a histogram of photopeak counts as a function of radial bin, displayed in Fig. 3.

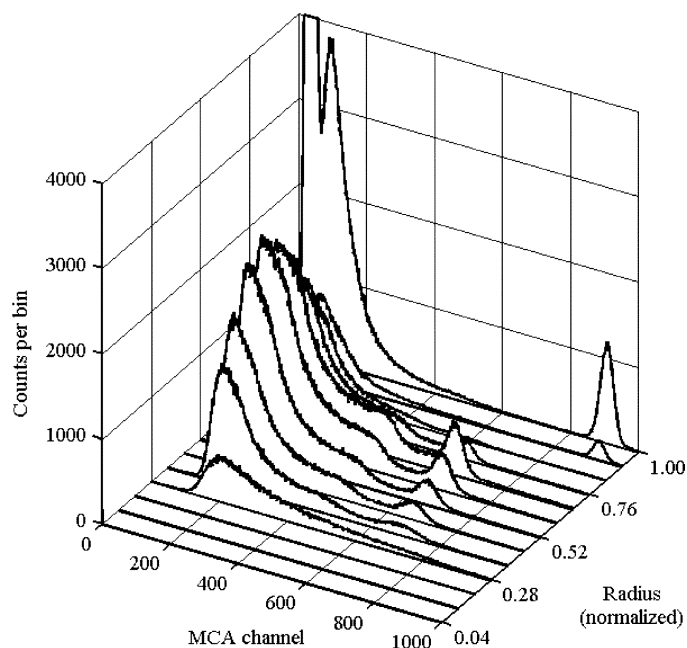


Fig. 2. Experimental ¹³⁷Cs radially-separated pulse-height spectrum. The peaks centered near channel 900 are test pulses.

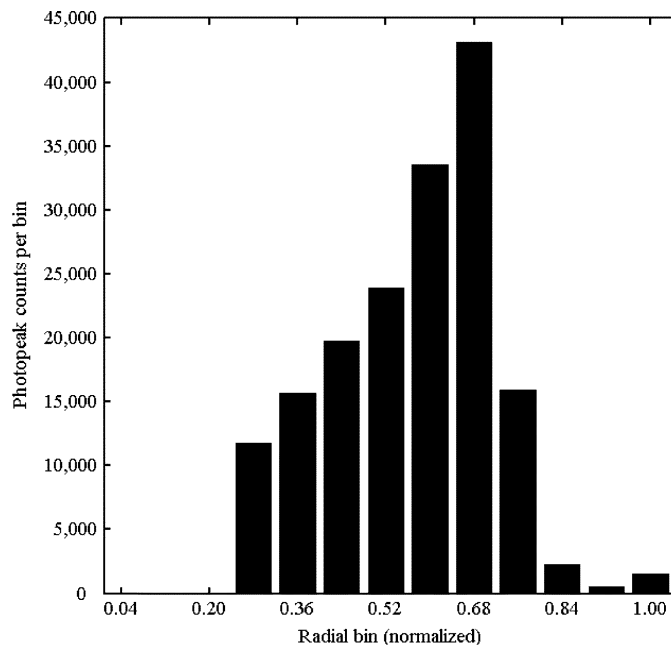


Fig. 3. Radial distribution of experimental ¹³⁷Cs photopeak counts.

In this histogram, it is evident that the photopeak count rate increases with radius, as is expected in a cylindrical geometry. Clearly, the photopeaks are confined to radial values between approximately 0.25 and 0.75, indicating that either the electric field is not sufficient to collect events from the entire volume or that the experimental data is being compressed into a smaller range of radial values than expected theoretically. This issue and others can be illuminated by simulations, so further discussion will be resumed in the Simulations section.

One powerful use of the radial sensing technique can be demonstrated now. In Fig. 2, the photopeak centroid actually

drifts slowly to lower channels as the radius increases. The centroids can be aligned manually to slightly improve the energy resolution of the overall energy spectrum. In addition, one can assume that properly-measured counts can only appear in radial bins that contain photopeaks: radial bins outside this range contain improperly-measured events, such as those with incomplete charge collection. If we select only events registering in proper radii, apply a photopeak alignment gain, and subtract out the measured background, the overall spectrum's energy resolution and peak-to-total count ratio improve noticeably, as demonstrated in Fig. 4. Quantitatively, the energy resolution of the ^{137}Cs photopeak improves from 87 channels to 66 channels FWHM, which is much closer to the electronic noise limit measured with a test pulse of 50 channels FWHM.

IV. SIMULATIONS

The detector simulations incorporate Monte Carlo methods with electrostatic simulations to create the best possible model of the detector response. The Maxwell 3-D [14] electrostatic solver has been used to simulate the operating electric field and weighting potential distributions within the detection volume. These results have been used, along with electron drift velocity data [15] and electron cloud dimensions [10], to simulate preamplifier waveforms. By randomly generating events within the detector, preamplifier sum and difference waveforms can be simulated, along with the Gaussian-shaped signal amplitudes. This information can be used to compare the true interaction position with the radius calculated using (5).

Fig. 5 shows this data, with the true interaction location on the abscissa and the radius calculated via signal amplitudes on the ordinate. In this figure, we immediately notice a plateau at small radii. Due to the nature of the summed anode signal, events occurring at radii inside the anode structure appear to be located at a normalized radius near 0.25, which is where the anode wires are physically located. Secondly, outside the anode wires, the slope of this scatter plot is linear through a radius of about 0.5, but then a considerable curvature of the data is present for large radii. This effect is due to the long rise time of the summed signal for events occurring near the cathode, which results in significant ballistic deficit of the shaped signal amplitude. Notice that nearly all events generate a computed radius between 0.25 and 0.75, which corresponds nicely with the range of experimental photopeak counts as displayed in Fig. 3. Finally, for any given true radius, there is a range of computed radii, which is due to the variation in weighting potential as a function of azimuthal angle within the detector. Events drifting directly toward a noncollecting anode wire can even produce unexpectedly large values of the computed radius, which is due to charge collection on the noncollecting wire. Despite this variation, the majority of computed radii lie in a narrow band that monotonically increases with true event radius, which allows the radial sensing method to be successfully employed.

The waveform simulations can be combined with Geant4 [16] Monte Carlo simulations to provide the most detailed model of detector response achievable. In these simulations, the physical geometry is recreated as accurately as possible. In addition to tracking energy deposition within the sensitive volume of the

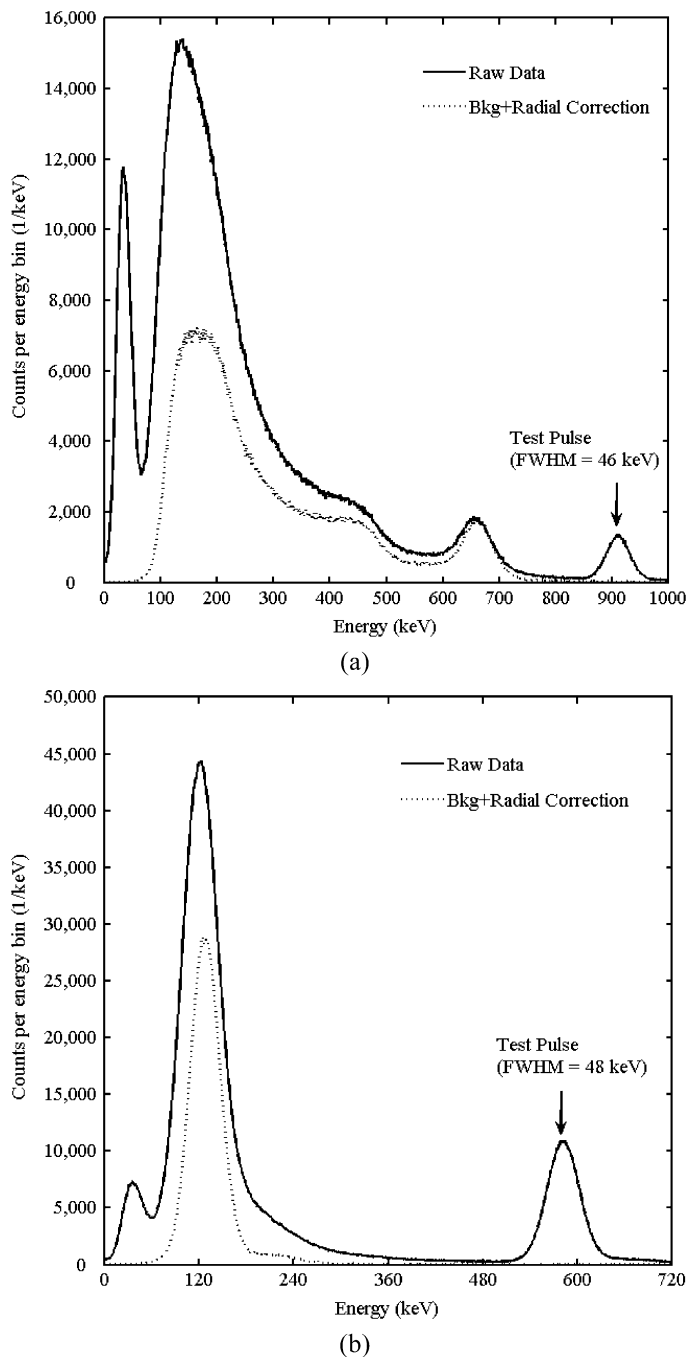


Fig. 4. The effects of background correction, event selection, and photopeak alignment upon experimental data. (a) ^{137}Cs source. (b) ^{57}Co source.

detector, these simulations also consider Fano statistics, waveform generation and shaping, and electronic noise. The resulting radially-separated spectrum for a simulated ^{137}Cs source is presented in Fig. 6.

Fig. 6 has much in common with the experimental data of Fig. 2. The lack of photopeak counts at normalized radii less than 0.25 and greater than about 0.75 is found in both figures; this is due to a weighting potential effect at small radii and ballistic deficit for events with long rise times. The photopeak resolution improvement as radius increases is seen clearly in the experimental and simulated data; this effect can be attributed to

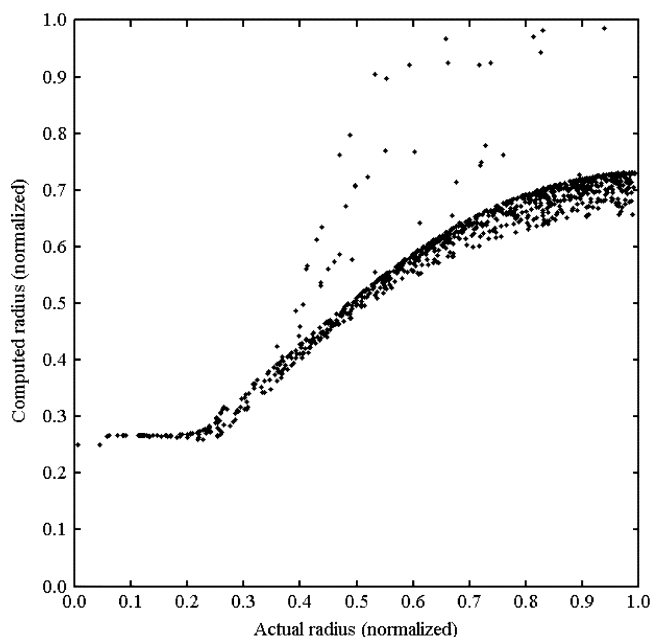


Fig. 5. Computed radius versus true radius in waveform simulations.

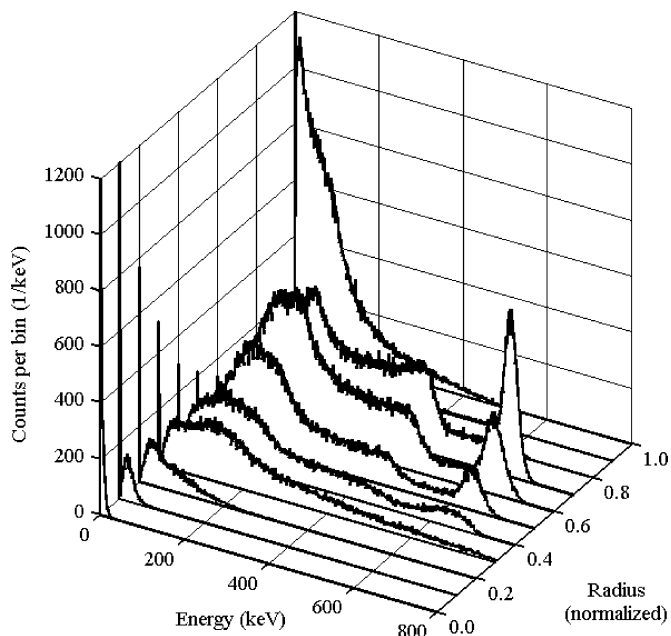


Fig. 6. Simulated radially-separated ^{137}Cs energy spectrum.

the azimuthal nonuniformity of the weighting potential near the anodes. A prominent low-energy continuum at computed radii ≥ 1.00 is also seen in both plots; this is largely due to electrons being collected at a noncollecting anode wire, which results in reduced pulse amplitudes coupled with artificially-large calculated event radii.

V. CONCLUSION

This paper presented a relatively simple method for determining the interaction radius of gamma rays within a HPXe detector. A simple theoretical approximation was derived, along

with an expression describing the relative position uncertainty. Experiments and detailed simulations generally were in good agreement qualitatively.

This technique has many practical applications for HPXe detectors. A simple application of radial sensing was presented that enhanced the collected energy spectrum by rejecting events registering in unphysical radii and aligning the photopeaks as a function of radial position. As another example, the purity of the xenon gas can be tested by checking for a decrease in photopeak amplitude as event radius increases. A third application could be to test for appropriate biasing of the detector by checking for registered events throughout the entire detection volume.

ACKNOWLEDGMENT

The authors thank the U.S. Department of Energy NEER program and the National Science Foundation Graduate Research Fellowship Program for financial support of this project. Also, Dr. L. J. Meng and D. Xu of the University of Michigan were of great assistance in setting up the digital pulse acquisition system.

REFERENCES

- [1] G. Tepper and J. Losee, "High resolution room temperature ionization chamber xenon gamma radiation detector," *Nucl. Instrum. Meth. A*, vol. 356, no. 2-3, pp. 339-346, Mar. 1995.
- [2] G. J. Mahler, B. Yu, G. C. Smith, W. R. Kane, and J. R. Lemley, "A portable gamma-ray spectrometer using compressed xenon," *IEEE Trans. Nucl. Sci.*, vol. 45, no. 3, pp. 1029-1033, Jun. 1998.
- [3] A. Bolotnikov and B. Ramsey, "Improving the energy resolution of high-pressure Xe cylindrical ionization chambers," *IEEE Trans. Nucl. Sci.*, vol. 44, no. 3, pp. 1006-1010, Jun. 1997.
- [4] G. L. Troyer, B. D. Keele, and G. C. Tepper, "Pulse rise-time characterization of a high pressure xenon gamma detector for use in resolution enhancement," *J. Radio. Nucl. Chem.*, vol. 248, no. 2, pp. 267-271, May 2001.
- [5] J. L. Lacy, A. Athanasiades, N. N. Shehad, L. Sun, T. D. Lyons, C. S. Martin, and L. Bu, "Cylindrical high pressure xenon spectrometer using scintillation light pulse correction," in *IEEE Nucl. Sci. Symp. Conf. Record*, Rome, Italy, 2004, vol. 1, pp. 16-20.
- [6] N. G. Goleminov, B. U. Rodionov, and V. Yu. Chepel, "Position-sensitive xenon gamma-quantum detector," *Instr. Exp. Tech.*, vol. 29, no. 2, pp. 325-328, Sep. 1986.
- [7] A. Athanasiades, J. L. Lacy, C. S. Martin, R. A. Austin, N. N. Shehad, and L. Sun, "Position sensing in a cylindrical ionization detector with a resistive cathode," *Nucl. Instrum. Meth. A*, vol. 505, no. 1-2, pp. 252-255, Jun. 2003.
- [8] A. Athanasiades, J. L. Lacy, and L. Sun, "Position sensing in a cylindrical ionization detector through use of a segmented cathode," in *IEEE Nucl. Sci. Symp. Conf. Record*, San Diego, CA, 2001, vol. 2, pp. 1151-1155.
- [9] P. N. Luke, "Single-polarity charge sensing in ionization detectors using coplanar electrodes," *Appl. Phys. Lett.*, vol. 65, no. 22, pp. 2884-2886, Nov. 1994.
- [10] S. D. Kiff, Z. He, and G. C. Tepper, "A new coplanar-grid high-pressure xenon gamma-ray spectrometer," *IEEE Trans. Nucl. Sci.*, vol. 52, no. 6, pp. 2932-2939, Dec. 2005.
- [11] Z. He, "Review of the Shockley-Ramo theorem and its application in semiconductor gamma-ray detectors," *Nucl. Instrum. Meth. A*, vol. 463, no. 1-2, pp. 250-267, May 2001.
- [12] *LabVIEW*. Austin, TX, USA: National Instruments, 2003, ver. 7.
- [13] *MATLAB*. Natick, MA, USA: The MathWorks, 2004, ver. 7.0.
- [14] *Maxwell 3D*. Pittsburgh, PA, USA: Ansoft Corp., 2003, ver. 9.
- [15] J. L. Pack, R. E. Voshall, and A. V. Phelps, "Drift velocities of slow electrons in krypton, xenon, deuterium, carbon monoxide, carbon dioxide, water vapor, nitrous oxide, and ammonia," *Phys. Rev.*, vol. 127, no. 6, pp. 2084-2089, Sep. 1962.
- [16] *Geant4*. Geneva, Switzerland: CERN, 2005, ver. 4.7.